ELECTRONIC SUPPLEMENTARY INFORMATION

Unveiling new [1+1] Schiff-base macrocycles towards high energy-barrier hexagonal bipyramidal Dy(III) single-molecule magnets

Alexandros S. Armenis,[a] Arpan Mondal,[b] Sean R. Giblin,[c] Catherine P. Raptopoulou,[d] Vassilis Psycharis,[d] Dimitris I. Alexandropoulos,[a] Jinkui Tang,[e] Richard A. Layfield*[b] and Theocharis C. Stamatatos*[a]

[a] *Department of Chemistry, University of Patras, Patras 26504, Greece. E-mail: thstama@upatras.gr; tel.: +30-2610996730.*

[b] *Department of Chemistry, School of Life Sciences, University of Sussex, Brighton BN1 9QR, U.K. E-mail: R.Layfield@sussex.ac.uk*

[c] *School of Physics and Astronomy, Cardiff University, Cardiff CF24 3AA, U.K.*

[d] *Institute of Nanoscience and Nanotechnology, NCSR "Demokritos", Aghia Paraskevi Attikis 15310, Greece.*

[e] *State Key Laboratory of Rare Earth Resource Utilization, Changchun Institute of Applied Chemistry, Chinese Academy of Sciences, Changchun 130022, P. R. China.*

Table of Contents

1. Materials and Physical Measurements

All experiments were carried out under aerobic conditions using materials and solvents as received without further purification. Elemental analyses (C, H, N) were performed by the University of Patras microanalytical service. DC and AC magnetic susceptibility measurements were performed using a Quantum Design MPMS-XL7 and a Quantum Design MPMS3 SQUID (up to frequencies of 1 kHz) magnetometers, respectively. AC susceptibility measurements up to 1 MHz were performed using a bespoke coil set integrated into the bore of a Quantum Design PPMS. Samples were prepared by gently crushing the crystalline materials before transferring them to a 7 mm NMR tube and covering them in eicosane. Then the tubes were flame-sealed under a static vacuum. The eicosane was melted in a water bath at 40 °C to prevent crystallite torquing. Diamagnetic corrections were performed using Pascal's constants.[1]

2. Synthesis and Structural Characterization

$[Dy(L^{N6})(Ph_3SiO)_2](PF_6)$ (**1-L^{N6}**): 2,6-Diacetylpyridine (0.20 mmol, 0.032 g), tetraethylenepentamine (0.20 mmol, 0.038 mL), and $DyCl_3 \cdot 6H_2O$ (0.20 mmol, 0.075 g) were transferred to a round bottom flask containing 15 mL of methanol resulting in a clear yellow solution. The mixture was refluxed for 24 hours giving an orange-colored clear solution and then the solvent was removed under reduced pressure yielding an oily precipitate. Then, to the residue was added a CH_2Cl_2 solution (15 mL) containing Ph_3SiOH

(0.80 mmol, 0.222 g) and Et_3N (0.80 mmol, 0.112 mL), and subsequently a H_2O solution (15 mL) containing NH_4PF_6 (0.20 mmol, 0.032 g), creating two layers. The reaction mixture was refluxed for 1 hour and the yellow, almost clear CH_2Cl_2 phase was separated with a separating funnel and then filtered giving a clear yellow solution. Pale yellow plate-like crystals suitable for single-crystal X-ray diffraction were isolated after 2-3 days by layering the CH_2Cl_2 solution with hexane. The crystals were collected by filtration, washed with CH_2Cl_2 (2 × 2 mL), and dried in air. The yield was 41% (based on Dy). The air-dried solid was analyzed as **1-L^{N6}**. Anal. Calcd for $C_{53}H_{58}DyF_6N_6O_2PSi_2$: C, 54.19; H, 4.98; N, 7.15. Found: C, 54.22; H, 4.84; N, 7.08.

[Dy(L^{N3O3})(Ph$_3$SiO)$_2$](PF$_6$) (1-L^{N3O3}): 2,6-Diacetylpyridine (0.20 mmol, 0.032 g), 1,11-diamino-3,6,9-trioxaundecane (0.20 mmol, 0.030 mL), and $Dy(NO_3)_3{\cdot}5H_2O$ (0.20 mmol, 0.088 g), were transferred to a round bottom flask containing 15 mL of methanol resulting in a yellow cloudy solution. The mixture was refluxed for 24 hours giving an orange/yellow colored cloudy solution and then the solvent was removed under reduced pressure yielding an orange/yellow solid. Then, to the residue was added a CH_2Cl_2 solution (15 mL) containing Ph_3SiOH (0.80 mmol, 0.222 g) and Et_3N (0.80 mmol, 0.112 mL), and subsequently a H_2O solution (15 mL) containing KPF_6 (0.20 mmol, 0.036 g), creating two layers. The reaction mixture refluxed for 1 hour and the pale yellow cloudy CH_2Cl_2 phase was separated with a separating funnel and then filtered giving a clear pale-yellow solution. Colorless plate-like crystals suitable for single-crystal X-ray diffraction were isolated after 2-3 days by layering the CH_2Cl_2 solution with Et_2O. The crystals were collected by filtration, washed with CH_2Cl_2 (2 × 2 mL), and dried in air. The yield was 36% (based on Dy). The air-dried solid was analyzed as **1-L^{N3O3}**. Anal. Calcd for $C_{53}H_{55}DyF_6N_3O_5PSi_2$: C, 54.05; H, 4.71; N, 3.57. Found: C, 54.03; H, 4.73; N, 3.55.

X-Ray Crystallographic details

Pale yellow crystals of **1-L^{N6}** (0.09 × 0.13 × 0.32 mm) were taken directly from the mother liquor and immediately cooled to 180 K. X-ray diffraction data were collected on a Rigaku R-AXIS SPIDER Image Plate diffractometer using graphite-monochromated Mo Kα (λ = 0.71073 Å) radiation. Data collection (ω-scans) and processing (cell refinement, data

reduction and empirical absorption correction) were performed using the CrystalClear program package.[2] The structure of **1-L^{N6}** was solved by direct methods using SHELXS ver. 2013/1[3] and refined by full-matrix least-squares techniques on F^2 with SHELXL ver. 2014/6.[4] The structure model was refined as a racemic twin. The SQUEEZE procedure[5] was applied for this compound and 2.5 dichloromethane molecules per formula of the asymmetric unit of the cell was estimated, based on the accessible solvent voids volume or electron counts within the voids per cell. The hydrogen atoms were introduced at calculated positions and refined as riding on their corresponding bonded atoms. All non-H atoms were refined anisotropically. Colorless crystals of **1-L^{N3O3}** (0.04 × 0.035 × 0.02 mm) were taken directly from the mother liquor and immediately cooled to 173 K. X-ray diffraction data were collected on a Bruker D8 VENTURE diffractometer using graphite-monochromated Cu Kα (λ = 1.54178 Å) radiation. The structure was solved using direct methods with SHELXT-2014[6] and refined by the full-matrix least-squares method based on F^2 with SHELXL-2014[4] through the OLEX2 interface.[7] The non-hydrogen atoms were successfully refined using anisotropic displacement parameters, and hydrogen atoms bonded to the carbon of the ligands were placed at their idealized positions using appropriate HFIX instructions in SHELXL. All atoms were included in subsequent refinement cycles in riding-motion approximation with isotropic thermal displacement parameters (U_{iso}) fixed at 1.2 or 1.5U_{eq} of the relative atom. Detailed information about crystal data and structure refinement for the complexes **1-L^{N6}** and **1-L^{N3O3}** is summarized in **Table S1**. Further crystallographic details can be found in the corresponding CIF files. Various figures of the structures were created, using Diamond 3 and Mercury software packages.[8,9]

Table S1. Crystallographic data for compounds **1-L^{N6}** and **1-L^{N3O3}**.

Parameter	**1-L^{N6}**	**1-L^{N3O3}**
Formula	$C_{54.25}H_{60.5}Cl_{2.5}DyF_6N_6O_2PSi_2$	$C_{53}H_{55}DyF_6N_3O_5PSi_2$
F_w / g·mol^{-1}	1280.86	1177.65
Crystal system	Monoclinic	Monoclinic
Space group	*Pn*	$P2_1/c$
a / Å	20.8869(6)	16.895(3)
b / Å	11.3031(4)	14.733(3)
c / Å	23.5314(8)	20.760(4)
α / °	90	90
β / °	98.892(1)	97.425(7)
γ / °	90	90
V / Å^3	5488.7(3)	5124.3(15)
Z	2	4
T / *K*	180.15	173.0
Radiation / λ (Å)	Mo Kα / 0.71073	Cu Kα / 1.54178
ρ_{calcd} / g cm^{-3}	1.550	1.526
Reflections collected/unique (R_{int})	102982/23012 (0.0593)	32297/8909 (0.0381)
Reflections with $I>2\sigma(I)$	20201	7878
No. of parameters	1280	642
R_1 [$I>2\sigma(I)$], wR_2 [$I>2\sigma(I)$][a,b]	0.0511, 0.1012	0.0306, 0.0836
R_1 (all data), wR_2 (all data)[a,b]	0.0630, 0.1087	0.0359, 0.0868
$(\Delta/\sigma)_{max}$	0.016	0.001
$\Delta\rho_{max}/\Delta\rho_{min}$ (e Å^{-3})	4.689/-4.070	0.458 /-1.320
CCDC number	2377131	2377167

[a] $R_1 = \Sigma(||F_o| - |F_o||) / \Sigma(|F_o|)$.
[b] $wR_2 = \{\Sigma[w(F_o^2 - F_c^2)^2] / \Sigma[w(F_o^2)^2]\}^{1/2}$, $w = 1 / [\sigma^2(F_o^2) + (aP)^2 + bP]$, where $P = [\max(F_o^2, 0) + 2F_c^2] / 3$.

Table S2. Continuous Shape Measures (CShM) values for the potential coordination polyhedra of the 8-coordinate Dy^{III} centers in complexes **1-L^{N6}** and **1-L^{N3O3}**.

Polyhedron[a,b]	Dy1 (**1-L^{N6}**)	Dy2 (**1-L^{N6}**)	**1-L^{N3O3}**
OP	33.60	32.58	31.56
HPY	20.67	21.77	21.57
HBPY	6.64	**4.53**	**1.61**
CU	7.77	5.69	9.17
SAPR	7.44	8.74	15.44
TDD	**4.86**	6.27	13.29
JGBF	7.29	6.83	6.53
JETBPY	24.68	22.00	23.57
JBTPR	6.01	7.68	14.38
BTPR	5.55	7.63	14.16
JSD	7.73	8.92	14.58
TT	8.57	6.54	9.91
ETBPY	22.33	20.65	21.04

[a] Abbreviations: OP, Octagon; HPY, Heptagonal pyramid; HBPY, Hexagonal bipyramid; CU, Cube; SAPR, Square antiprism; TDD, Triangular dodecahedron; JGBF, Johnson gyrobifastigium; JETBPY, Johnson elongated triangular bipyramid; JBTPR, Biaugmented trigonal prism; BTPR, Biaugmented trigonal prism; JSD, Snub diphenoid; TT, Triakis tetrahedron; ETBPY, Elongated trigonal bipyramid. [b] The value in boldface indicates the closest polyhedron according to the Continuous Shape Measures.

Table S3. Selected bond distances (Å) and angles (°) for complex **1-L^{N6}**.

Bond distances (Å)			
Dy1		**Dy2**	
Dy1-N1	2.586(9)	Dy2-N7	2.566(12)
Dy1-N2	2.525(8)	Dy2-N8	2.598(10)
Dy1-N3	2.514(8)	Dy2-N9	2.690(11)
Dy1-N4	2.548(9)	Dy2-N10	2.592(11)
Dy1-N5	2.713(9)	Dy2-N11	2.686(10)
Dy1-N6	2.588(8)	Dy2-N12	2.684(11)
Dy1-O1	2.194(6)	Dy2-O3	2.143(7)
Dy1-O2	2.196(7)	Dy2-O4	2.152(7)
Bond angles (°)			
Dy1		**Dy2**	
O1-Dy1-O2	158.8(2)	O3-Dy2-O4	168.6(3)
N1-Dy1-N2	63.1(3)	N7-Dy2-N8	63.7(4)
N2-Dy1-N3	63.8(3)	N8-Dy2-N9	62.0(3)
N3-Dy1-N4	66.7(3)	N9-Dy2-N10	62.5(3)
N4-Dy1-N5	65.5(3)	N10-Dy2-N11	65.5(3)
N5-Dy1-N6	63.4(3)	N11-Dy2-N12	63.1(3)
N6-Dy1-N1	66.5(3)	N12-Dy2-N7	64.6(4)
O2-Dy1-N1	83.0(3)	O3-Dy2-N7	89.3(4)
O2-Dy1-N2	82.4(3)	O3-Dy2-N8	87.4(3)
O2-Dy1-N3	82.0(3)	O3-Dy2-N9	89.3(3)
O2-Dy1-N4	81.6(3)	O3-Dy2-N10	80.6(3)
O2-Dy1-N5	127.6(3)	O3-Dy2-N11	114.9(3)
O2-Dy1-N6	82.0(3)	O3-Dy2-N12	75.9(3)
O1-Dy1-N1	89.4(3)	O4-Dy2-N7	85.9(4)
O1-Dy1-N2	76.5(3)	O4-Dy2-N8	81.2(3)
O1-Dy1-N3	86.8(3)	O4-Dy2-N9	85.1(3)
O1-Dy1-N4	110.3(3)	O4-Dy2-N410	105.3(3)

O1-Dy1-N5	73.5(3)	O4-Dy2-N11	76.5(3)
O1-Dy1-N6	112.9(3)	O4-Dy2-N12	111.1(3)

Table S4. Selected bond distances (Å) and angles (°) for complex **1-L^{N3O3}**.

Bond distances (Å)		**Bond angles (°)**	
Dy1-N1	2.587(2)	O4-Dy1-O1	175.84(8)
Dy1-N2	2.610(2)	N1-Dy1-N3	61.62(8)
Dy1-N3	2.562(2)	N3-Dy1-O3	61.75(7)
Dy1-O2	2.569(2)	O3-Dy1-O2	58.96(6)
Dy1-O3	2.576(2)	O2-Dy1-O5	59.73(6)
Dy1-O5	2.609(2)	O5-Dy1-N2	61.68(7)
Dy1-O1	2.147(2)	N2-Dy1-N1	61.36(7)
Dy1-O4	2.163(2)	O4-Dy1-N1	93.53(8)
		O4-Dy1-N3	80.41(8)
		O4-Dy1-O3	99.41(7)
		O4-Dy1-O2	96.10(7)
		O4-Dy1-O5	83.45(7)
		O4-Dy1-N2	92.41(8)
		O1-Dy1-O2	87.23(7)
		O1-Dy1-O3	84.45(7)
		O1-Dy1-N3	100.19(8)
		O1-Dy1-N1	83.21(7)
		O1-Dy1-N2	83.76(7)
		O1-Dy1-O5	96.13(7)

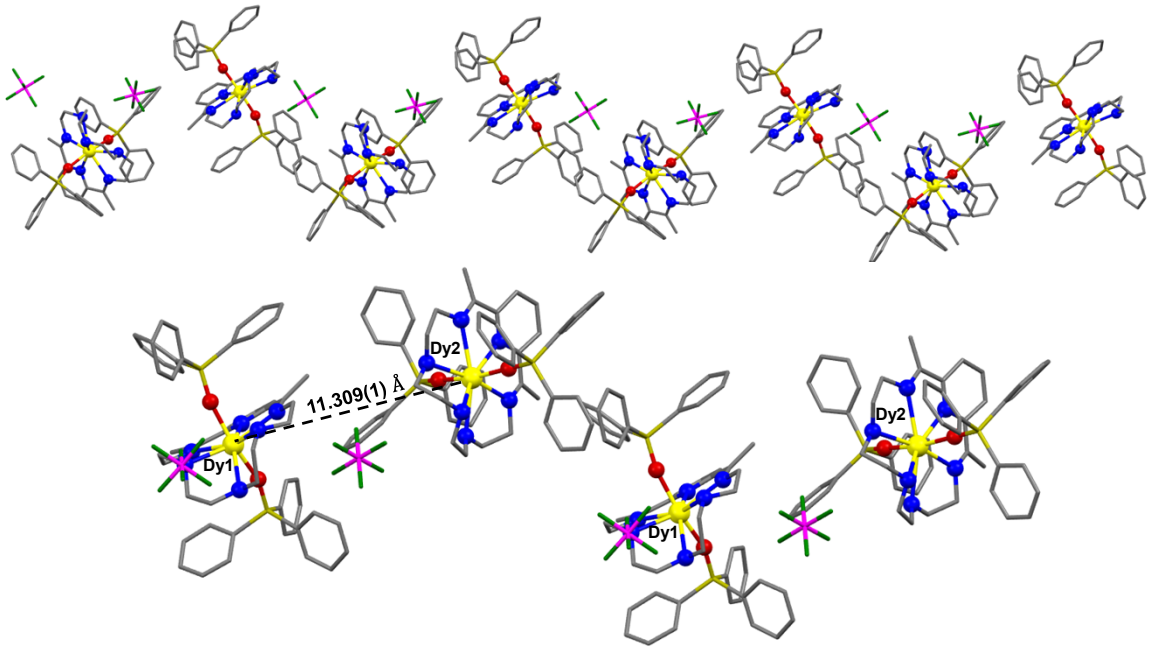

Fig. S1 (Top) A portion of the alternating sequence of the two crystallographically independent mononuclear complexes in the crystal of **1-L^{N6}** viewed along the *c*-axis. (Bottom) Visualization of the shortest intermolecular Dy···Dy distance (black dashed lines) in the crystal of **1-L^{N6}**. Color scheme: Dy^{III}, yellow; O, red; N, blue; C, grey; Si, olive; P, magenta; F, green. The Dy^{III} ions and the donor atoms (N and O) are illustrated as spheres. The CH_2Cl_2 solvate molecules and the H-atoms are omitted for clarity.

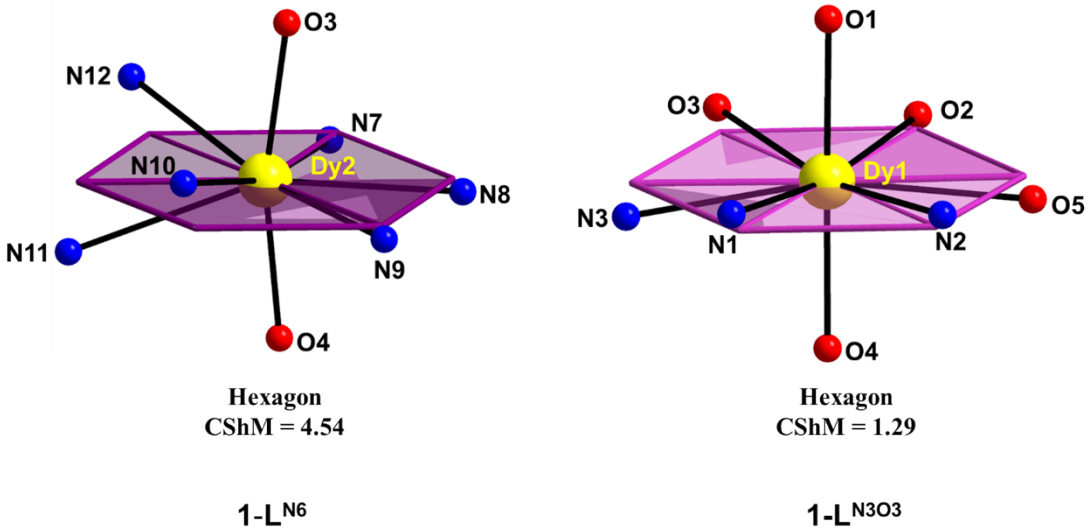

Fig. S2 Deviation of the equatorial donor atoms of the macrocyclic ligand **L^{N6}** (for Dy2) (left) and **L^{N3O3}** (right) in the corresponding complexes from the ideal hexagonal plane

highlighted with purple color. The CShM values according to SHAPE program are indicated. Color scheme: Dy^{III}, yellow; O, red; N, blue.

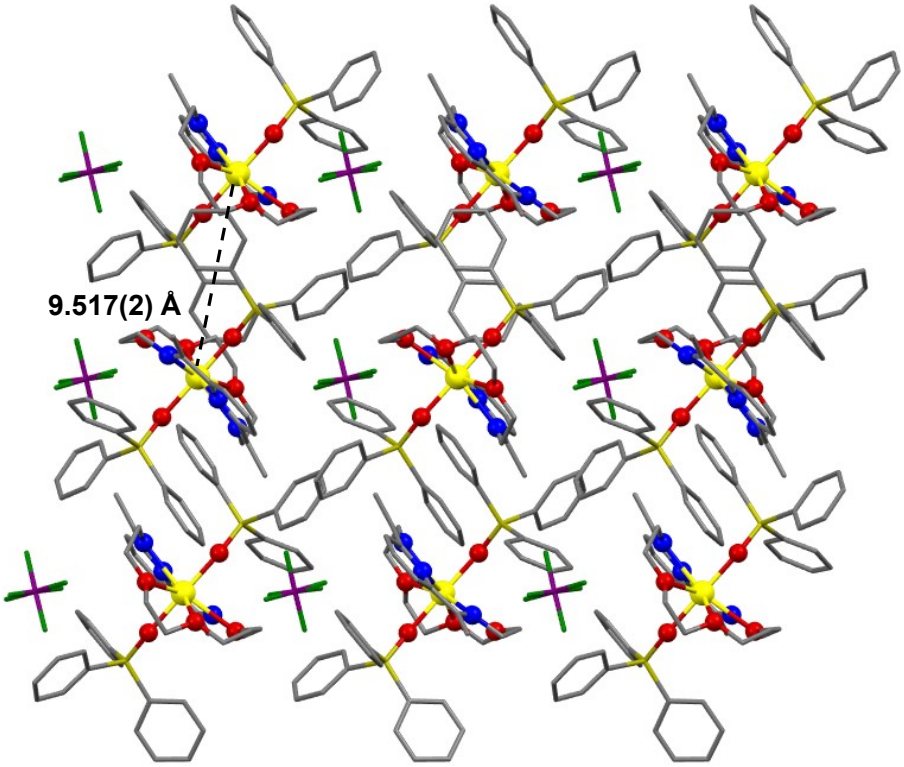

Fig. S3 A portion of the repeating monomeric complexes in the crystal of **1-L^{N3O3}** viewed along the *b*-axis and visualization of the shortest intermolecular Dy···Dy distance as black dashed lines. Color scheme: Dy^{III}, yellow; O, red; N, blue; C, grey; Si, olive; P, magenta; F, green. The Dy^{III} ions and the donor atoms (N and O) are illustrated as spheres. The H-atoms are omitted for clarity.

3. Magnetic Measurements

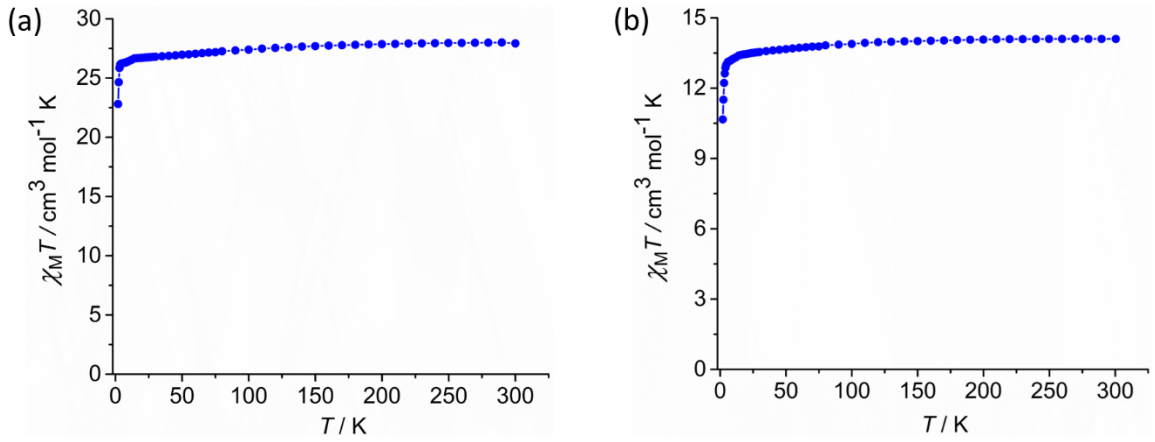

Fig. S4 $\chi_M T$ vs. T plots for complexes (**a**) **1-L^{N6}** and (**b**) **1-L^{N3O3}** under an applied *dc* field of 0.1 T. The solid lines are guides only.

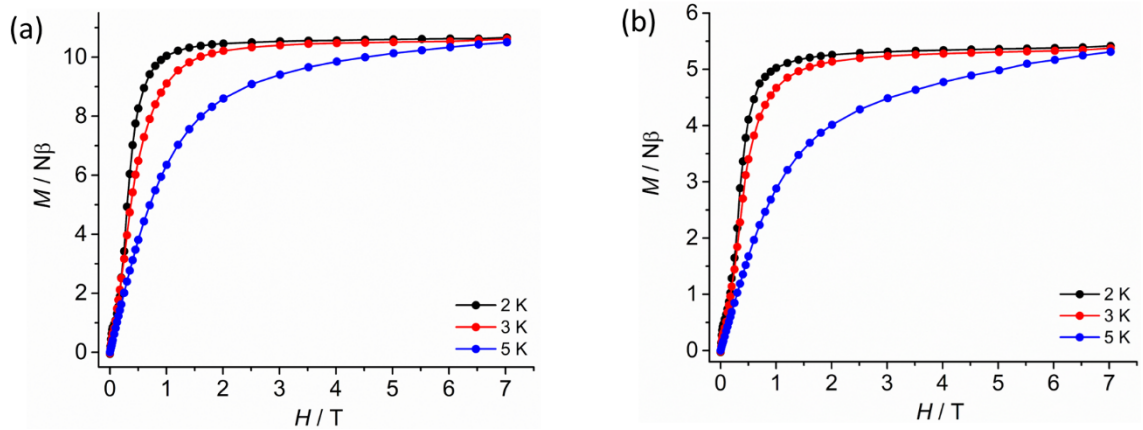

Fig. S5 Plots of magnetization (*M*) vs field (*H*) for complexes (**a**) **1-L^{N6}** and (**b**) **1-L^{N3O3}** at different low temperatures. The solid lines are guides only.

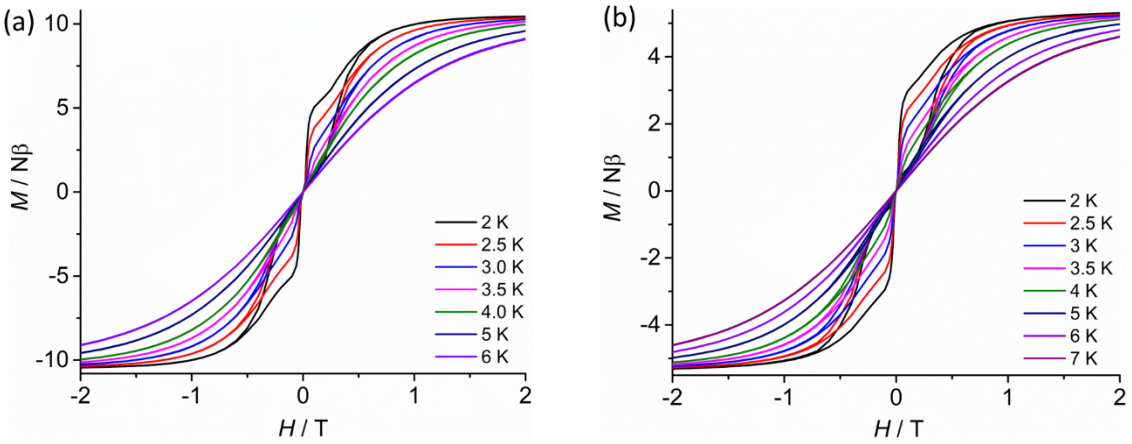

Fig. S6 Magnetic hysteresis loops for complexes (**a**) **1-L^{N6}** and (**b**) **1-L^{N3O3}** collected at different low temperatures (2.0-7.0) K with a mean field sweep rate of 31 Oe s^{-1}.

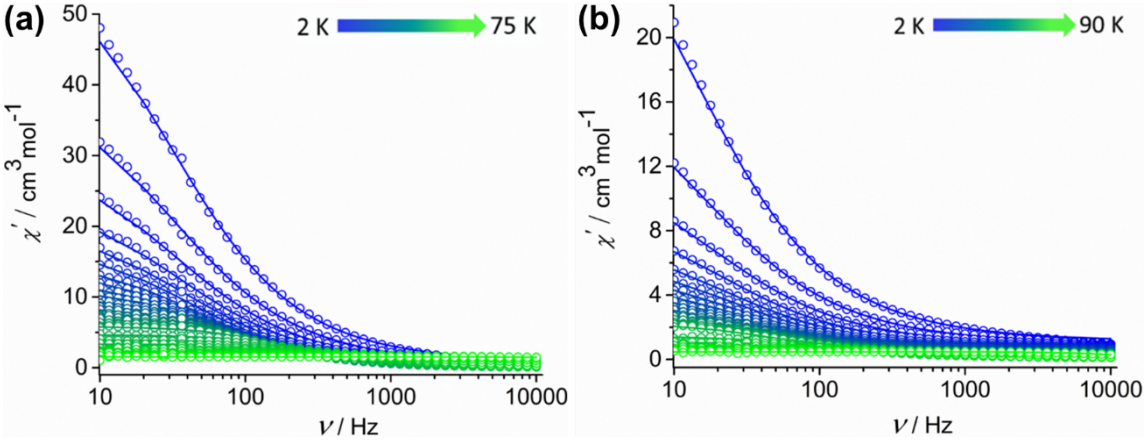

Fig. S7 (**a**) Frequency dependence of the in-phase (χ_M') magnetic susceptibility under zero applied *dc* field for complex **1-L^{N6}** over the temperature range 2-75 K. (**b**) Frequency dependence of the in-phase (χ_M') magnetic susceptibility under zero applied *dc* field for complex **1-L^{N3O3}** over the temperature range 2-90 K. Solid lines represent fits to the data.

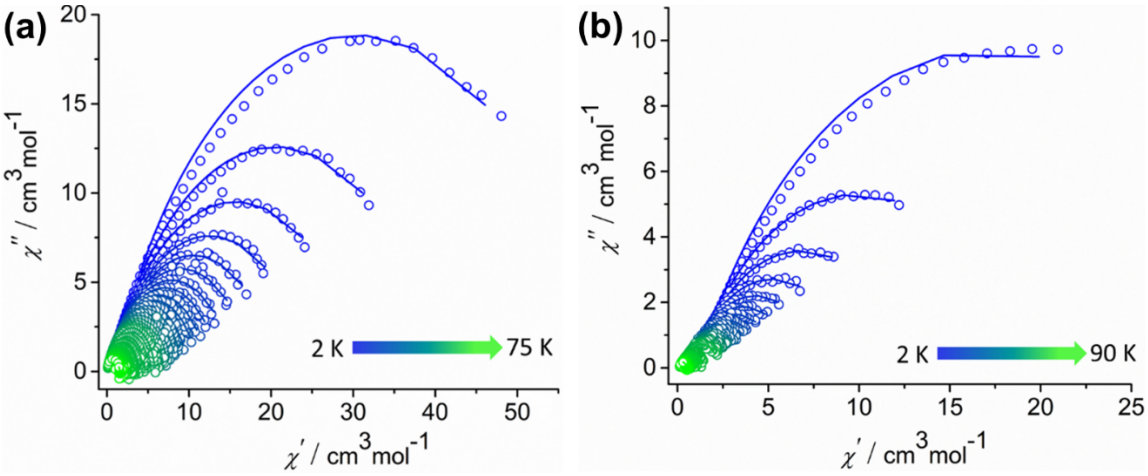

Fig. S8 (**a**) Cole-Cole plots for complex **1-L^{N6}** obtained from the *ac* susceptibility data in zero applied *dc* field at T = 2-75 K. (**b**) Cole-Cole plots for complex **1-L^{N3O3}** obtained from the *ac* susceptibility data in zero applied *dc* field at T = 2-90 K. Solid lines represent fits to the data using **Equations S1** and **S2**.[10] The parameters are listed in **Table S5** for **1-L^{N6}** and **Table S6** for **1-L^{N3O3}**.

$$\chi'(v) = \chi_S + \frac{(\chi_T - \chi_S)[1 + (2\pi v\tau)^{(1-\alpha)}\sin(\frac{\alpha\pi}{2})]}{1 + 2(2\pi v\tau)^{(1-\alpha)}\sin\left(\frac{\alpha\pi}{2}\right) + (2\pi v\tau)^{2(1-\alpha)}} \quad \textbf{(Equation S1)}$$

$$\chi''(v) = \frac{(\chi_T - \chi_S)(2\pi v\tau)^{(1-\alpha)}\cos(\frac{\alpha\pi}{2})}{1 + 2(2\pi v\tau)^{(1-\alpha)}\sin\left(\frac{\alpha\pi}{2}\right) + (2\pi v\tau)^{2(1-\alpha)}} \quad \textbf{(Equation S2)}$$

Table S5. Relaxation fitting parameters for complex **1-L^{N6}**.

T / K	χ_S / cm^3 mol^{-1}	χ_T / cm^3 mol^{-1}	τ / s	α
2	0.71146	60.27894	0.00494	0.28151
3	0.45029	40.87205	0.00489	0.29068
4	0.33708	31.05302	0.0048	0.29395
5	0.27295	24.76477	0.00446	0.29244
6	0.26428	20.81069	0.00417	0.2812

7	0.26945	17.87502	0.00378	0.26274
8	0.25449	15.54473	0.00348	0.24878
9	0.25114	13.81526	0.00306	0.22935
10	0.23042	12.37884	0.00269	0.21642
11	0.21784	11.2282	0.00237	0.20121
12	0.21523	10.00405	0.00203	0.18019
13	0.18996	9.33469	0.00189	0.17797
14	0.18507	8.63805	0.00168	0.16376
15	0.2016	7.90002	0.00146	0.1388
16	0.16642	7.52833	0.00138	0.14721
17	0.19094	6.93419	0.00119	0.11981
18	0.15997	6.50535	0.0011	0.12321
19	0.15692	6.16919	9.92019E-4	0.11528
20	0.17469	5.86423	8.96256E-4	0.09724
25	0.11071	4.66443	5.90956E-4	0.09993
30	0.08344	3.92381	4.07685E-4	0.10032
35	0.06652	3.3483	2.88128E-4	0.10132
40	0.07715	2.86326	2.04234E-4	0.07596
45	0.05107	2.57255	1.47479E-4	0.08898
50	0.04171	2.28745	9.83283E-5	0.09077
55	0.03601	2.09409	5.85598E-5	0.11597
60	0.11369	1.93507	3.1346E-5	0.13409
65	0.34368	1.77393	1.76642E-5	0.08696
70	0.46414	1.65644	8.74879E-6	0.05437
75	0.60226	1.54436	4.47341E-6	0.02269

Table S6. Relaxation fitting parameters for complex **1-L^{N3O3}**.

T / K	χ_S / cm^3 mol^{-1}	χ_T / cm^3 mol^{-1}	τ / s	α
2	1.12584	33.16993	0.01103	0.30594
3	0.97476	18.89586	0.0097	0.31881

4	0.8566	12.88243	0.00873	0.31573
5	0.76384	9.70494	0.00779	0.30539
6	0.67491	7.95775	0.00747	0.30625
7	0.62039	6.62126	0.00659	0.28958
8	0.56663	5.7534	0.00616	0.2821
9	0.52306	4.9953	0.00558	0.26889
10	0.48304	4.52825	0.00543	0.27056
11	0.45127	4.11007	0.00513	0.26271
12	0.42581	3.74901	0.00472	0.25255
13	0.39667	3.43137	0.0044	0.24892
14	0.37438	3.29006	0.00432	0.24785
15	0.35425	3.15668	0.00433	0.25018
16	0.33912	2.92443	0.00407	0.24536
17	0.31922	2.72724	0.00385	0.24795
18	0.31032	2.56477	0.00347	0.2283
19	0.29522	2.46125	0.00341	0.23511
20	0.28682	2.34266	0.00313	0.2202
30	0.20233	1.45287	0.00167	0.16164
40	0.16682	1.08141	9.81621E-4	0.11247
50	0.14246	0.85249	5.91777E-4	0.07611
60	0.12572	0.70788	3.52731E-4	0.05765
70	0.12013	0.61083	1.777E-4	0.05604
80	0.12173	0.53968	6.07293E-5	0.04174
90	0.12727	0.47028	1.56333E-5	0.01034

4. *Ab initio* calculations

Computational Details

All calculations were carried out on the coordinates obtained from the relevant crystal structure using the ORCA 5.0.2 software package.[11] The positions of hydrogen atoms were optimized at the DFT level using a pure GGA PBE exchange correlation functional, keeping the position of the other atoms constant.[12] To avoid the convergence problem, we replaced Dy^{3+} with Y^{3+} during the optimizations. The def2-TZVP basis sets with effective core potential (ECP) were used to treat the core electrons of yttrium throughout the DFT calculations.[13] In the multi-reference *ab initio* calculations, we used the DKH (Douglas-Kroll-Hess) Hamiltonian throughout to consider relativistic effects. The dysprosium centre was modelled with the SARC2-DKH-QZVP basis set, and all other atoms were treated with the DKH-def2-TZVP basis set in combination with the 'AutoAux' auxiliary basis set.[14] The active space CAS(7,9) was constructed from 9 electrons in 7 f-orbitals. In the configuration interaction procedure, 21 sextets, 128 quartets, and 130 doublets were computed for all the complexes. To consider the spin-orbit coupling, we also used the quasi-degenerate perturbation theory (QDPT) approach using SA-CASSCF wave functions.[15] The SINGLE_ANISO module as implemented in ORCA was used to compute the *g*-tensor and crystal field parameters of the low-lying excited states using previously calculated spin-orbit states.[16]

Table S7. SINGLE_ANISO computed crystal-field parameters for the studied complexes.

k	q	**1-L^{N6}**		**1-L^{N3O3}**
		Dy1	**Dy2**	
	-2	-0.8999E+00	0.8150E+00	-0.2796E+00
	-1	0.6849E+00	-0.3314E+00	0.1645E+00
2	0	-0.5228E+01	-0.7186E+01	-0.7349E+01
	1	-0.5229E+00	-0.1753E+00	-0.5121E+00
	2	-0.5543E+00	0.1140E+01	-0.2355E+00

	-4	0.7313E-02	-0.6043E-02	0.9647E-04
	-3	-0.3276E-01	-0.4700E-01	-0.1158E-01
	-2	-0.3763E-02	-0.2046E-02	-0.1302E-02
	-1	-0.4271E-02	0.3047E-02	-0.1849E-02
4	0	-0.1086E-01	-0.1379E-01	-0.14301E-01
	1	0.9020E-02	-0.1234E-02	0.2657E-02
	2	-0.7550E-02	-0.6227E-02	0.5750E-03
	3	-0.3477E-01	0.4144E-01	-0.5926E-02
	4	0.2619E-02	-0.5309E-02	-0.6408E-03
	-6	0.5510E-03	-0.5933E-03	0.2675E-04
	-5	0.7132E-03	0.1148E-03	-0.3647E-04
	-4	0.5573E-04	-0.3276E-04	0.1038E-04
	-3	-0.6159E-04	-0.1721E-03	-0.5582E-04
	-2	-0.7343E-05	-0.3092E-04	-0.8395E-05
	-1	-0.6385E-05	-0.1883E-04	0.1536E-04
6	0	0.2717E-04	0.4904E-04	0.4996E-04
	1	-0.9242E-04	0.4592E-04	0.1530E-04
	2	0.8810E-05	-0.2920E-04	0.2008E-05
	3	-0.8785E-04	0.1592E-03	0.1018E-05
	4	0.1323E-04	-0.3884E-04	0.4604E-05
	5	0.1132E-03	-0.1085E-03	-0.9179E-04
	6	0.9516E-05	-0.5509E-04	-0.6479E-03

The Hamiltonian used to calculate the crystal field parameters is the following:

$$\hat{H}_{CF} = \sum_{k=-q}^{q} B_q^k \hat{O}_q^k$$

where $\hat{O}_q^k$ = extended Stevens operators, k = rank of the ITO (2,4,6), q = the component of the ITO, = -k, -k+1, ... 0, 1, ... k.[17]

Table S8. *Ab initio* calculated low-lying spin-orbit energy states for the investigated complexes.

1-L^{N6}		**1-L^{N3O3}**
Dy1	**Dy2**	

0.000	0.000	0.000
0.000	0.000	0.000
384.1643	481.3223	499.0064
384.1643	481.3223	499.0064
670.2686	880.9037	910.3601
670.2686	880.9037	910.3601
806.6027	1108.4679	1152.4641
806.6027	1108.4679	1152.4641
862.2454	1146.6523	1218.2777
862.2454	1146.6523	1218.2777
924.3683	1221.1437	1240.2093
924.3683	1221.1437	1240.2093
961.6702	1299.9197	1297.2875
961.6702	1299.9197	1297.2875
1031.1669	1373.5719	1381.6221
1031.1669	1373.5719	1381.6221

Table S9. Single_aniso computed energy of the KDs, *g*, angle between the anisotropic axis of the excited states with the ground state (°), and wavefunctions composition for **1-L^{N6}** (**Dy1**).

Kramers doublets (KDs)	Energy (cm^{-1})	g_x	g_y	g_z	angle (°)	Wave function composition
1	0.000	2.1×10^{-3}	2.4×10^{-3}	19.83		99.7%|±15/2>
2	384.164	0.162	0.182	16.89	1.08	98.44%|±13/2>
3	670.269	0.161	0.564	13.31	5.25	90.50%|±11/2>+4.96%|±1/2>+2.07%|±7/2>
4	806.603	3.892	5.339	10.84	74.16	41.68%|±9/2>+7.58%|±7/2>+12.90%|±5/2>+32.23%|±3/2>+4.73%|±1/2>
5	862.245	0.082	4.971	11.64	77.75	0.39%|±13/2>+2.65%|±11/2>+19.75%|±9/2>+16.58%|±7/2>+13.37%|±5/2>+0.88%|±3/2>+46.31%|±1/2>
6	924.368	12.00	6.721	0.054	11.04	0.41%|±13/2>+4.54%|±11/2>+2.80%|±9/2>+21.39%|±7/2>+27.43%|±5/2>+18.17%|±3/2>+25.19%|±1/2>
7	961.670	2.693	5.353	8.572	77.92	29.87%|±9/2>+10.97%|±7/

						2>+3.23%|±5/2>+38.48%|±3/2>+16.73%|±1/2>
8	1031.167	1.130	3.226	15.71	100.58	4.86%|±9/2>+41.04%|±7/2>+41.40%|±5/2>+9.75%|±3/2>+1.67%|±1/2>

Table S10. Magnitudes of transition magnetic moment matrix elements (in Bohr magneton) calculated for **1-L^{N6} (Dy1**).

Climbing Transition			Crossing Transition		
Initial KD	Final KD	Magnitude	Initial KD	Final KD	Magnitude
1	2	1.765	1	1	7.6×10^{-4}
1	3	0.1087	1	2	2.6×10^{-3}
1	4	0.05431	1	3	0.02529
1	5	0.06919	1	4	0.04943
1	6	0.06030	1	5	0.03324
1	7	0.05196	1	6	0.03058
1	8	0.02867	1	7	0.03603
2	3	2.382	1	8	0.04751
2	4	0.12502	2	2	0.05752
2	5	0.2661	2	3	0.08928
2	6	0.2805	2	4	0.2041
2	7	0.1805	2	5	0.2518
2	8	0.08321	2	6	0.2072
3	4	2.468	2	7	0.09554
3	5	1.371	2	8	0.09668
3	6	0.7164	3	3	0.1347
3	7	0.9200	3	4	0.5460
3	8	0.2644	3	5	0.8147
4	5	1.808	3	6	0.5280
4	6	1.139	3	7	0.3561

4	7	0.8999	3	8	0.2316
4	8	0.4525	4	4	2.4424
5	6	1.667	4	5	2.1726
5	7	1.547	4	6	0.9246
5	8	0.4033	4	7	1.064
6	7	2.080	4	8	0.2819
6	8	0.7869	5	5	1.190
7	8	2.426	5	6	0.9744
			5	7	1.235
			5	8	1.117
			6	6	1.380
			6	7	1.589
			6	8	1.288
			7	7	2.003
			7	8	1.411
			8	8	1.543

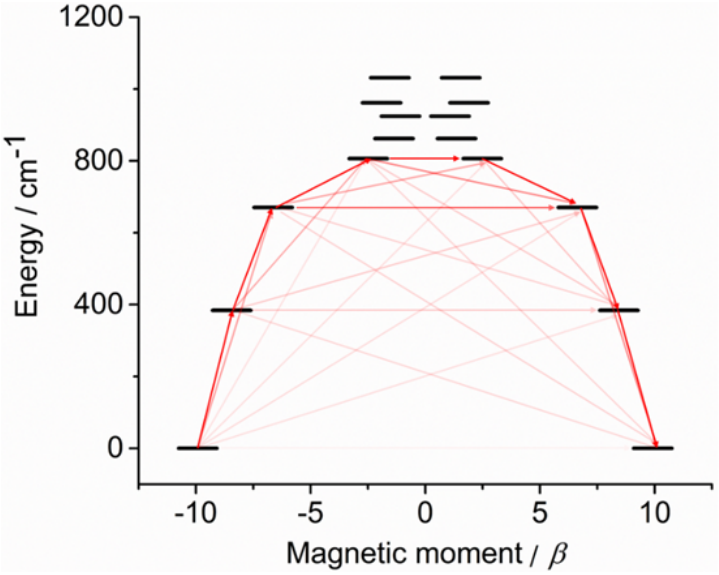

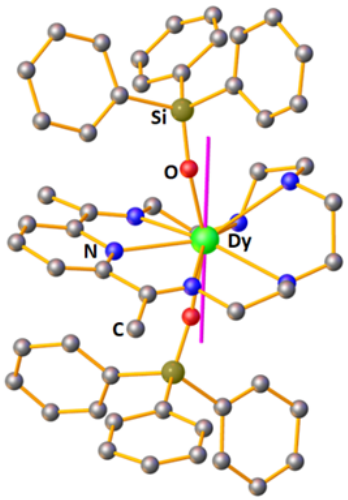

Fig. S9 (left) Single_aniso computed energy of the KDs for complex **1-L^{N6}** (**Dy1**). Dark red arrows show the most probable relaxation route and light red arrows indicate less significant but non-negligible matrix elements between states. (right) The orientation of the ground state anisotropic axis (purple rod).

Table S11. Single_aniso computed energy of the KDs, *g*, angle between the anisotropic axis of the excited states with ground state (°), and wavefunctions composition for **1-L^{N6} (Dy2**).

Kramers doublets (KDs)	Energy (cm^{-1})	g_x	g_y	g_z	angle (°)	Wave function composition
1	0.000	2.9×10^{-4}	5.5×10^{-4}	19.85		99.85%|±15/2>
2	481.322	0.081	0.089	16.92	0.74	99.33%|±13/2>
3	880.904	0.344	0.480	13.71	0.74	95.73%|±11/2>+2.40%|±1/2>
4	1108.468	4.250	5.869	7.701	71.20	48.17%|±9/2>+4.90%|±7/2>+3.23%|±5/2>+0.86%|±3/2>+33.08%|±1/2>
5	1146.652	0.940	3.468	13.95	76.47	2.17%|±11/2>+16.32%|±9/2>+0.63%|±7/2>+16.98%|±5/2>+9.82%|±3/2>+53.92%|±1/2>
6	1221.144	0.850	3.200	11.63	90.66	20.72%|±9/2>+46.57%|±7/2>+23.80%|±5/2>+5.37%|±3/2>+3.15%|±1/2>
7	1299.920	0.107	1.420	16.64	91.29	1.16%|±11/2>+9.98%|±9/2>+4.29%|±7/2>+13.84%|±5/2>+42.82%|±3/2>+27.69%|±1/2>
8	1373.572	1.004	3.124	15.49	87.20	4.56%|±9/2>+42.82%|±7/2>+40.81%|±5/2>+8.79%|±3/2>+2.25%|±1/2>

Table S12. Magnitudes of transition magnetic moment matrix elements (in Bohr magneton) calculated for **1-L^{N6} (Dy2**).

Climbing Transition			Crossing Transition		
Initial KD	Final KD	Magnitude	Initial KD	Final KD	Magnitude
1	2	1.771	1	1	1.4×10^{-4}
1	3	0.09743	1	2	7.3×10^{-3}
1	4	0.06203	1	3	0.01124
1	5	0.05146	1	4	0.03076
1	6	0.01824	1	5	0.02158
1	7	0.04660	1	6	0.04313
1	8	0.03220	1	7	0.03268
2	3	2.388	1	8	0.04055
2	4	0.1012	2	2	0.02852
2	5	0.2008	2	3	0.04292
2	6	0.1361	2	4	0.08187
2	7	0.1518	2	5	0.1935
2	8	0.1316	2	6	0.04547
3	4	2.412	2	7	0.1413
3	5	1.235	2	8	0.04765
3	6	0.2990	3	3	0.1382
3	7	0.559	3	4	0.2725
3	8	0.2198	3	5	0.5269
4	5	2.406	3	6	1.007
4	6	2.079	3	7	0.4297
4	7	0.9800	3	8	0.3384
4	8	0.4198	4	4	2.126
5	6	1.875	4	5	0.7762
5	7	0.9360	4	6	1.2780
5	8	0.7078	4	7	1.005
6	7	0.6213	4	8	0.2727
6	8	1.505	5	5	1.280
7	8	1.599	5	6	1.131

			5	7	0.7594
			5	8	0.3341
			6	6	2.571
			6	7	0.6931
			6	8	1.654
			7	7	2.753
			7	8	1.995
			8	8	2.911

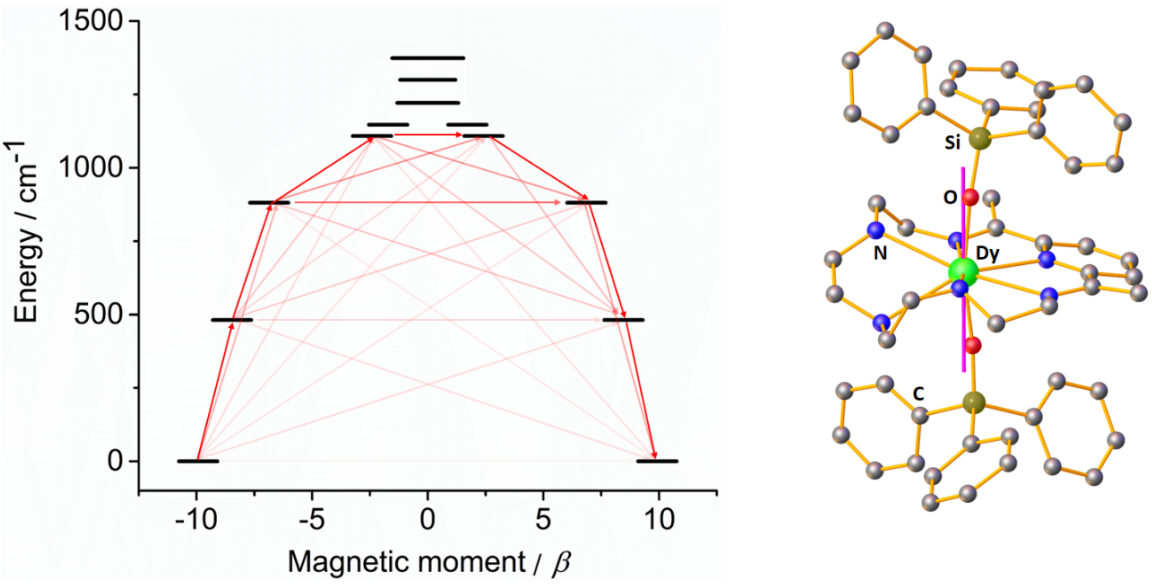

Fig. S10 (left) Single_aniso computed energy of the KDs for complex **1-L^{N6}** (**Dy2**). Dark red arrows show the most probable relaxation route and light red arrows indicate less significant but non-negligible matrix elements between states. (right) The orientation of the ground state anisotropic axis (purple rod).

Table S13. Single_aniso computed energy of the KDs, *g*, angle between the anisotropic axis of the excited states with the ground state (°), and wavefunctions composition for **1-L^{N3O3}**.

Kramers doublets	Energy (cm^{-1})	g_x	g_y	g_z	angle (°)	Wave function composition

(KDs)						
1	0.000	4.6×10^{-4}	4.8×10^{-4}	19.86		99.96%|±15/2>
2	499.006	0.096	0.099	16.94	0.78	99.69%|±13/2>
3	910.360	0.058	0.180	13.75	2.03	96.73%|±11/2>+2.93%|±1/2>
4	1152.464	1.272	2.709	6.620	7.75	66.31%|±9/2>+1.01%|±7/2>+30.92%|±3/2>+0.86%|±1/2>
5	1218.278	9.662	7.637	1.083	1.32	2.63%|±11/2>+1.67%|±9/2>+5.79%|±7/2>+9.75%|±5/2>+0.55%|±3/2>+79.39%|±1/2>
6	1240.209	0.709	5.516	11.24	94.33	0.34%|±11/2>+2.08%|±9/2>+40.16%|±7/2>+41.20%|±5/2>+1.58%|±3/2>+14.56%|±1/2>
7	1297.287	0.046	1.030	4.55	86.60	29.23%|±9/2>+1.03%|±7/2>+1.72%|±5/2>+66.12%|±3/2>+1.81%|±1/2>
8	1381.622	11.69	7.723	1.613	6.61	51.93%|±7/2>+46.55%|±5/2>+0.77%|±3/2>+0.17%|±1/2>

Table S14. Magnitudes of transition magnetic moment matrix elements (in Bohr magneton) calculated for **1-L^{N3O3}**.

Climbing Transition			Crossing Transition		
Initial KD	Final KD	Magnitude	Initial KD	Final KD	Magnitude
1	2	1.770	1	1	1.5×10^{-4}
1	3	0.04292	1	2	5.6×10^{-4}
1	4	0.01558	1	3	0.01358
1	5	0.03357	1	4	0.02346
1	6	0.02190	1	5	0.008197
1	7	0.02138	1	6	0.03082
1	8	0.01120	1	7	0.02682
2	3	2.388	1	8	0.03038
2	4	0.07369	2	2	0.03260
2	5	0.1442	2	3	0.04809
2	6	0.08565	2	4	0.1016

2	7	0.06560	2	5	0.2265
2	8	0.02431	2	6	0.08589
3	4	2.6069	2	7	0.1085
3	5	0.5165	2	8	0.00933
3	6	0.3856	3	3	0.0422
3	7	0.9313	3	4	0.1024
3	8	0.07393	3	5	0.5434
4	5	1.024	3	6	0.3200
4	6	2.589	3	7	0.3610
4	7	1.439	3	8	0.09147
4	8	0.5086	4	4	0.6977
5	6	1.178	4	5	1.837
5	7	1.252	4	6	1.357
5	8	0.4561	4	7	0.5507
6	7	1.117	4	8	0.1280
6	8	1.172	5	5	2.853
7	8	2.961	5	6	1.260
			5	7	2.484
			5	8	0.5328
			6	6	2.141
			6	7	0.9883
			6	8	1.0189
			7	7	1.039
			7	8	1.434
			8	8	2.882

5. Additional data and plots

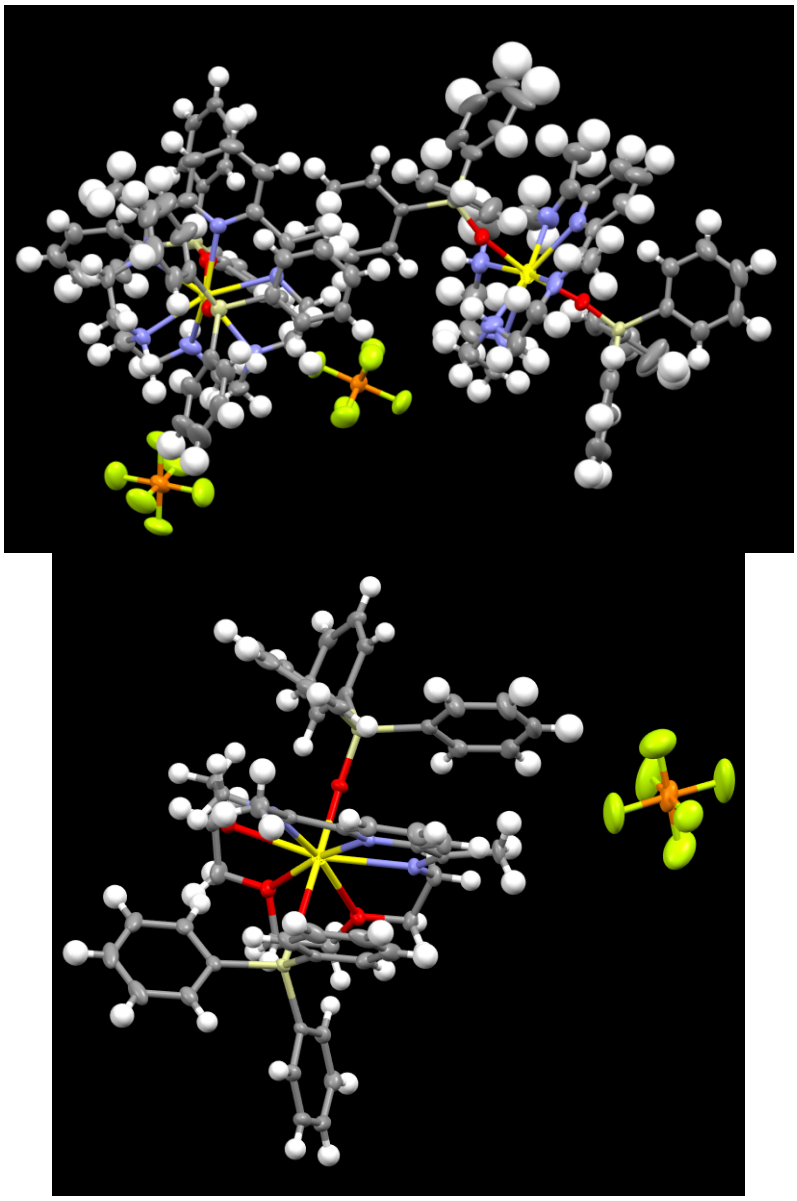

Fig. S11 ORTEP representations of complexes **1-L^{N6}** (top) and **1-L^{N3O3}** (bottom); thermal ellipsoids are at the 30% probability level.

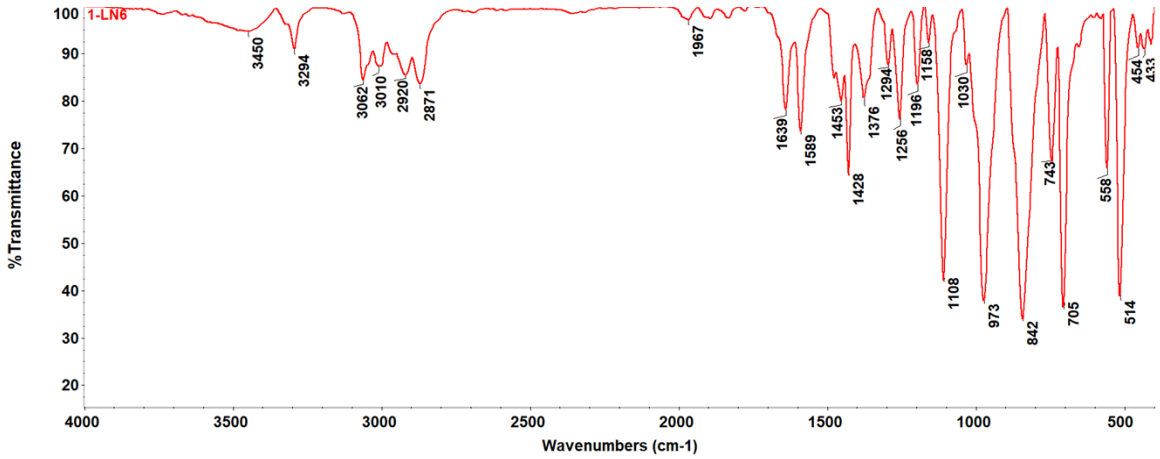

Fig. S12 FT-IR (KBr, cm^{-1}) spectrum of the compound **1-L^{N6}**.

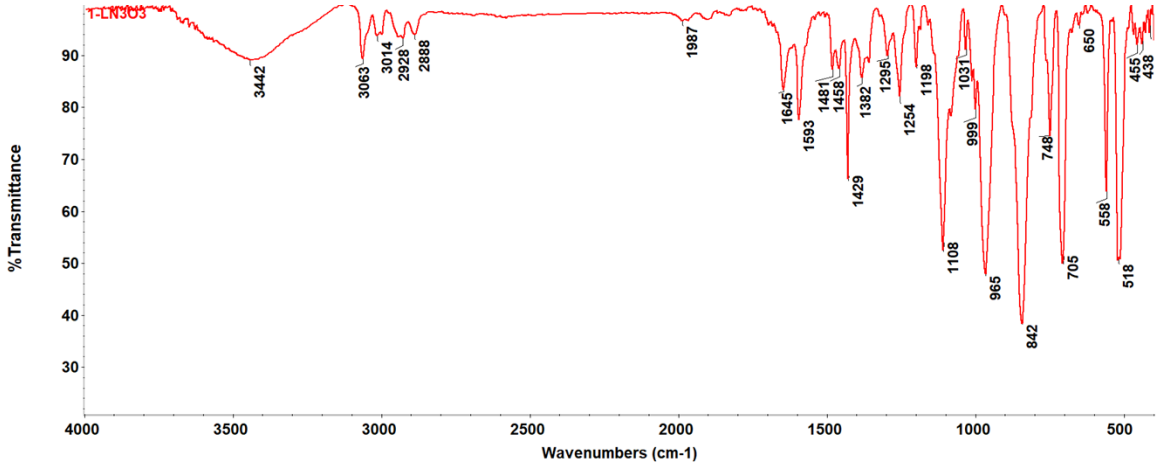

Fig. S13 FT-IR (KBr, cm^{-1}) spectrum of the compound **1-L^{N3O3}**.

6. References

[1] G. A. Bain, J. F. Berry, *J. Chem. Ed.* 2008, **85**, 532-536.

[2] *CrystalClear*, Rigaku/MSC Inc., The Woodlands, TX, USA, 2005.

[3] G. M. Sheldrick, *Acta Crystallogr., Sect. A: Fundam. Crystallogr.*, 2008, **64**, 112.

[4] G. M. Sheldrick, *Acta Crystallogr., Sect. C: Struct. Chem.*, 2015, **C71**, 3−8.

[5] A. L. Spek, *Acta Crystallogr., Sect. C: Cryst. Struct. Commun.*, 2015, **71**, 9.

[6] G. M. Sheldrick, *Acta Crystallogr., Sect. A: Found. Adv.*, 2015, **A71**, 3−8.

[7] O. V. Dolomanov, L. J. Bourhis, R. J. Gildea, J. A. K. Howard and H. Puschmann, *J. Appl. Crystallogr.*, 2009, **42**, 339–341.

[8] K. Brandenburg, *DIAMOND*, *Release 3.1f*, Crystal Impact GbR, Bonn, Germany, 2008.

[9] J. Bruno, J. C. Cole, P. R. Edgington, M. K. Kessler, C. F. Macrae, P. McCabe, J. Pearson and R. Taylor, *Acta Crystallogr., Sect. B: Struct. Sci.*, 2002, **58**, 389–397.

[10] J. Tang and P. Zhang, *Lanthanide Single Molecule Magnets*, Springer Berlin Heidelberg, Berlin, Heidelberg, 2015.

[11] F. Neese, F. Wennmohs, U. Becker and C. Riplinger, *J. Chem. Phys.*, 2020, **152**, 224108.

[12] (*a*) J. P. Perdew, K. Burke and M. Ernzerhof, *Phys. Rev. Lett.*, 1997, **78**, 1396-1396. (*b*) J. P. Perdew, K. Burke and M. Ernzerhof, *Phys. Rev. Lett.*, 1996, **77**, 3865-3868.

[13] (*a*) A. Schäfer, H. Horn and R. Ahlrichs, *J. Chem. Phys.,* 1992, **97**, 2571-2577. (*b*) F. Weigend and R. Ahlrichs, *Phys. Chem. Chem. Phys.*, 2005, **7**, 3297-3305.

[14] (*a*) D. Aravena, F. Neese and D. A. Pantazis, *J. Chem. Theory Comput.*, 2016, **12**, 1148-1156. (*b*) J. Chmela and M. E. Harding, *Mol. Phys.*, 2018, **116**, 1523-1538.

[15] D. Ganyushin and F. Neese, *J. Chem. Phys.*, 2006, **125**, 024103.

[16] L. F. Chibotaru and L. Ungur, *J. Chem. Phys.*, 2012, **137**, 064112.

[17] (*a*) K. W. H. Stevens, *Rep. Prog. Phys.*, 1967, **30**, 189–226. (*b*) K. W. H. Stevens, *Proc. Phys. Soc. A*, 1952, **65**, 209–215.